

Microfiber-coupler-assisted control of wavelength tuning for Q-switched fiber laser with few-layer molybdenum disulfide nanoplates

JIN-HUI CHEN,¹ GUO-QING DENG,² SHAO-CHENG YAN,¹ CHENG LI,¹ KAI XI,^{2,3} FEI XU,^{1,*} AND YAN-QING LU¹

¹College of Engineering and Applied Sciences, Nanjing University, Nanjing 210093, China

²School of Chemistry & Chemical Engineering, Nanjing University, Nanjing 210093, China

³e-mail: kaixi@nju.edu.cn

*Corresponding author: feixu@nju.edu.cn

Received 2 June 2015; revised 6 July 2015; accepted 7 July 2015; posted 8 July 2015 (Doc. ID 241980); published 27 July 2015

Based on the liquid exfoliated method, we obtained the few-layer molybdenum disulfide (MoS₂) nanoplates solution. By thermal evaporation method, we directly deposited MoS₂ thin film onto the facet of a fiber patch cord. The modulation depth of the film is as high as 29%, and a Q-switched fiber laser was achieved. We also provided a new method to continuously tune the output laser with a tuning sensitivity of ~5.5 nm/(1% strain) by controlling the cavity loss with a strained microfiber coupler (MFC). © 2015 Optical Society of America

OCIS codes: (060.0060) Fiber optics and optical communications; (140.3510) Lasers, fiber.

<http://dx.doi.org/10.1364/OL.40.003576>

The great success of graphene [1–3] has inspired researchers to explore other two-dimensional (2D) materials with either similar or distinct properties. Among the family of the emerging 2D materials, a group of transition metal dichalcogenides (TMDs) such as molybdenum disulfide (MoS₂) has stood out for their distinctive electronic and opto-electronic properties. Like graphene, the TMDs have strong intra-layer bonding and weak Van Der Waals force between layers. As a result, it is easy to peel off bulky TMDs to obtain few-layer structures or even the monolayer limit simply by tape-based micromechanical exfoliation [4]. Interestingly, the 2D nature of TMDs is fundamentally different from their bulk counterpart. It is well known that the bulk MoS₂ is an indirect semiconductor with band gap 1.29 eV, while the monolayer MoS₂ becomes a direct semiconductor with the band gap increased to 1.80 eV because of lateral quantum confinement [5,6]. The inherent inversion symmetry broken of monolayer MoS₂ combined with spin-orbit coupling (SOC) of *d* orbitals of Mo leads to coupled spin and valley physics [7], which has been experimentally demonstrated recently [8,9]. For nonlinear optics, the broken inversion symmetry of atomically thin monolayer MoS₂ has shown

strong second-harmonic generation (SHG) [10,11] in contrast to its centrosymmetric bulk counterpart. Furthermore, it is found that there exists edge state with resonantly enhanced second-harmonic generation that can be attributed to the translation symmetry breaking at the edge of 2D crystal [12]. Also, similar to graphene, the few-layer MoS₂ shows broadband saturable absorption effects as a result of lattice defects [13] or edge states [14]. Recently, a number of groups have reported Q-switched fiber laser [13–15] or mode-locked fiber laser [16–19] based on few-layer MoS₂, which unambiguously indicates MoS₂ can be applied to pulse fiber laser.

Pulse fiber lasers have wide applications ranging from material processing to scientific research. The emerging 2D materials like graphene [20], black phosphorus [21], topological insulator [22,23], and TMDs have been proved to be promising for ultrafast optics. The saturation threshold of MoS₂ is much less than other 2D materials, which indicates that it is easier to achieve pulse fiber laser with MoS₂. Here we also report a tunable Q-switched fiber laser by liquid exfoliated few-layer MoS₂. Different from previous work, for example, few-layer MoS₂ was coated on a microfiber [17,19], the saturable absorber (SA) of MoS₂ film is directly deposited onto the facet of optical fiber by thermal evaporation of solute, and a high-modulation depth of ~29% has been achieved. It provides a cost-effective way to combine SA into the fiber circuit. Besides, we use a microfiber coupler (MFC) to extract the laser power and simultaneously in-line tune the wavelength of the output fiber laser. By precisely controlling the strain of MFC, we can continuously change the wavelength-dependent coupling efficiency of the MFC [24]. As a result, we can dynamically control the cavity loss at different wavelengths, and thus change the lasing wavelengths. In our experiment, we achieved continuous tuning from 1550 to 1575 nm with a tuning sensitivity of ~5.5 nm/(1% strain). By further optimizing the structure of MFC, we believe this method can easily cover the whole gain spectrum, and it can also expand to other optical bands. Although there are numerous methods to obtain tunable fiber lasers, for example grating [25], fiber birefringence [26],

tunable filter [14,15], etc., these techniques are either bulky, or complicated or even not continuously tunable. The mechanical tuning method proposed here is for the first time, as far as we know, implemented to tune pulse fiber-laser wavelength. We believe our technique may pave the way to the in-line tunable *Q*-switched fiber laser.

Ionic intercalation induced exfoliation of TMDs dates back to the 1970s [27], and monolayers of MoS₂ were obtained by a similar technique [28]. An improved chemical Li-intercalation and exfoliation method for the synthesis of MoS₂ nanosheets were employed in this work as schematically shown in Figs. 1(a)–1(e). Typically, 1 g MoS₂ bulk crystals (99%, Alfa Aesar) were put into a 50-mL teflon-lined autoclave, filled with 10-mL *n*-Butyllithium (*n*-BuLi) solution of *n*-hexane (Aladdin). After heating the autoclave at 100°C for 4 h, the solution was shifted to a 50-mL three-necked bottle and kept magnetic stirring for 48 h at 25°C under nitrogen atmosphere. The Li-intercalated MoS₂ powder was collected by filtration and rinsed with *n*-hexane to eliminate the residual *n*-BuLi. Then the Li-intercalated MoS₂ powder was added into 600-mL deionized water and kept sonication for 4 h to exfoliate MoS₂ powder to nanosheets. Afterward, the resulting suspensions were centrifuged for 15 min at 1500 rpm to separate the centrifugate and supernatant. Then the supernatant were centrifuged for 30 min at 8000 rpm for 3 times, achieving another centrifugate. After deionized-water washing for 3–5 times by centrifugation, this centrifugate was dispersed into 500-mL deionized water by sonication for 1 h to prepare MoS₂ nanosheets suspension. Finally, 2-Mercaptoethylamine (C₂H₇N₂, 95% adamas-beta) was used to modify the MoS₂ nanosheets to reduce lattice defects and stabilize the solution.

The Raman characterization is a useful method to determine the thickness of 2D materials. Figure 2(a) demonstrates the typical Raman spectra of the fabricated few-layer MoS₂ deposited on SiO₂/Si substrate. The E_{2g}¹ peak is ~383.3 cm⁻¹, and A_{1g} peak is ~405.4 cm⁻¹. Thus the energy difference between the two modes is 22.1 cm⁻¹, which indicates that the layer number is 2–3 [29,30]. We also collected the Raman spectra of the deposited MoS₂ film of different spatial positions, and the calculated energy difference varied from 22 to 24 cm⁻¹, which meant that the layer numbers of the MoS₂ were among 2–5. The nature of chemical exfoliation method determines that the thickness of nanoflakes of MoS₂ is dispersive.

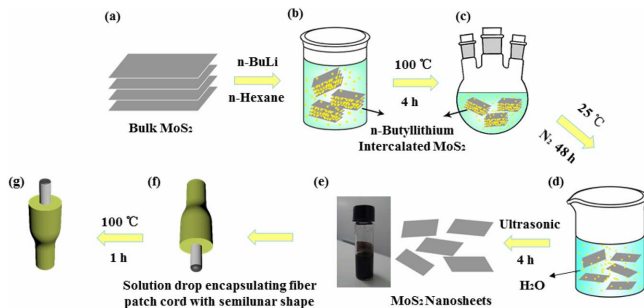


Fig. 1. Fabrication process of MoS₂ on an optical fiber. Panels (a)–(e) illustrate how to produce liquid exfoliated MoS₂ nanoplates. Panels (f), (g) show the thermal evaporation solute method to deposit thin film of MoS₂ onto the fiber patch cord.

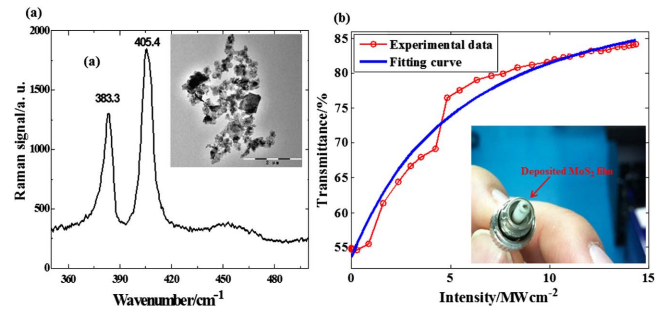


Fig. 2. Characterization of the MoS₂ film. (a) The Raman spectra of the as-fabricated few-layer MoS₂. The inset is TEM image of few-layer MoS₂. The scale bar is 2 μm. (b) Nonlinear transmission profile shows saturable absorption of SA. The inset is the camera image of the MoS₂ deposited on the facet of patch cord.

Considering the 0.62-nm interlayer spacing of a single layer of the S-Mo-S [29], the thickness of MoS₂ is 1.2–3.1 nm. From TEM characterization, as illustrated in the inset of Fig. 2(a), we find that the sizes of MoS₂ flakes vary from several hundreds of nanometers to sub-micrometers, and the typical size is ~500 nm.

In the past few years, researchers have explored many methods to employ the liquid-exfoliated 2D materials into the fiber ring cavity, such as polymer composite [14,16], optical trapping method [18], microfiber evanescent wave interaction [17,19], etc. Here thermal evaporation of the solute-induced deposition method was proposed as a more convenient way to obtain thin film on the facet of fiber patch cord, as illustrated in Figs. 1(f) and 1(g). First, we put the head of fiber patch cord upside down and fixed it by a scaffold. After that, a drop of MoS₂ solution was attached onto the facet of it. The gravity and surface tension of the drop would induce a semilunar-like structure, which encapsulated the facet of patch cord. Finally, we heated the sample in an oven with 100°C for an hour to evaporate the solute. And a thin film of MoS₂ was naturally created as shown in Fig. 2(b).

We utilize a similar technique [17] to characterize saturation property of the as fabricated SA. The duration time of input pulse laser (SPL, APFL-1550-B-CUSTOM) is 10 ns with a repetition frequency of 1 MHz. We can see from Fig. 2(b) that the modulation depth of the SA is 29%. We fit the experimental data with a model combined with a saturable absorption and two photon absorption (TPA) effects [18]:

$$T = \exp\left(-\frac{\alpha_0 L}{1 + I/I_s} - \beta I L\right), \quad (1)$$

where α_0 is the linear absorption coefficient, I is the input intensity, I_s is the saturable intensity, β is the TPA coefficient, and L is the thickness of the deposited film. From the fitting curves, we find that I_s , $\alpha_0 L$, βL are 4.53 MW/cm², 63% and 0.1%/MW cm⁻², respectively. The TPA contribution is negligible as expected [18]. We also find that when the injected power intensity is higher than 20 MW/cm², the sample will suffer irreversible damage. There are several factors to influencing the optical damage threshold of the MoS₂-saturable absorber (SA), such as the flakes' thickness, quality of flakes,

heat dissipation rate, etc., and the optical damage threshold can be further improved either by polymer composite or integrating MoS₂ with microfiber [17].

An MFC was fabricated from two standard optical fibers (SMF-28, Corning, New York, USA) using the flame brushing technique [24], as shown in Fig. 3(a). And the inset in Fig. 3(a) demonstrates a typical microscopic image of the fabricated MFC with the diameter $\sim 10\ \mu\text{m}$. We utilized a super-continuum source (NKT K91-120-02) to characterize the output spectrum of MFC, as illustrated in Fig. 3(b). Since the MFC is fixed at the translational stages (Newport, XML 350), we can inline stretch the MFC by controlling the movement of the translational stage, and the blue shift of the spectrum of MFC was observed, which is clearly demonstrated in Fig. 3(c). It is because the refractive index and coupling length of MFC vary with the strain [24]. The shifting spectrum of MFC indicates that it can serve as a tunable filter by inserting it into a fiber-laser circuit. There may be a concern that tuning MFC by strain will introduce strong fiber birefringence or polarization effect into the fiber circuit. According to the relatively thick MF employed here and theoretical calculations, we find that the birefringence of MFC is small. As a result, it can be expected that the MFC will not have evident polarization effect. It should be noted that in order to avoid multi-wavelength lasing (we will talk it in detail later), the free spectrum range (FSR) of the MFC should be larger than the gain bandwidth. That is to say, for an erbium-doped fiber laser, the FSR of as-fabricated MFC needs to be larger than 40 nm. From Fig. 3(b), we can see that the MFC meets the requirement.

Previous experiment shows that the as fabricated SA has relatively high modulation depth. To further demonstrate that it can be applied to pulse laser generation, we inserted the deposited-film patch cord into a fully fiber-integrated ring cavity (Fig. 4). The cavity consisted of 7.5-m EDF (Nufern, EDFC-980-HP C-band), a polarization-independent isolator to ensure unidirectional propagation, and a polarization controller. Notably, we employed an MFC to extract laser power and simultaneously tuned the lasing wavelength by stretching. The effective coupling ratio is around 2.5:1, as indicated by Fig. 3(b).

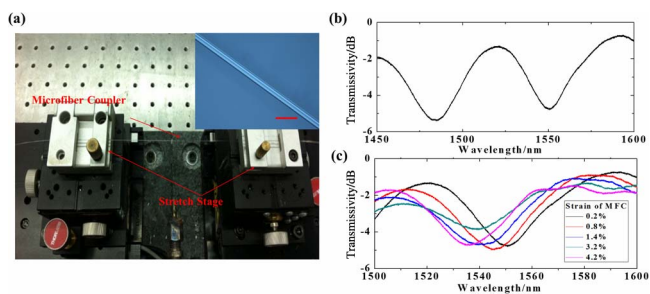


Fig. 3. Fabrication of MFC and stretching MFC measurement. (a) The camera image of as fabricated MFC fixed at the translational stages, which also serves as stretching stages in later experiment. The inset is the microscopic image of the MFC. The scale bar is $50\ \mu\text{m}$. (b) A typical output spectrum of MFC launched by a super-continuum source. (c) The blue shift of output spectrum of MFC as the strain increased.

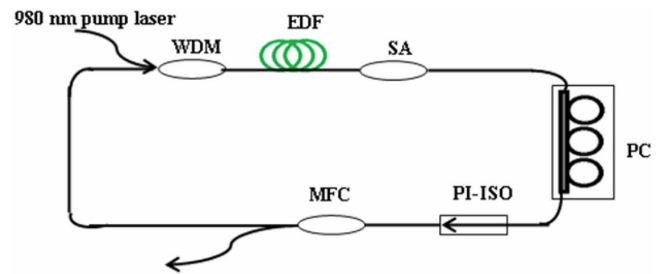


Fig. 4. Schematic of the erbium-doped Q-switched fiber laser by the MoS₂ SA. WDM, wavelength division multiplexer; EDF, erbium-doped fiber; PC, polarization controller; PI-ISO, polarization-independent isolator; and MFC, microfiber coupler.

As the input pump power (OPEAK, Pump-LSB-980-500-SM) increased, we observed the output laser experiencing from continuous-wave to self-started pulse train. Figure 5(a) illustrates typical time-domain pulse train with pump power at 60 mW. The pulse signal was probed by a photo-detector (New Focus, 1544-B) and monitored by an oscilloscope (Agilent Technologies, DSO-X 4024A). The inset in Fig. 5(a) shows the corresponding RF spectrum of output pulse with resolution bandwidth (RBW) 100 Hz. The peak-to-pedestal extinction is as high as 40 dB (10^4 contrast), indicating pulse stability. The average output power varies from 0.5 to 3.5 mW, while the pulse duration time is varied from $\sim 35\ \mu\text{s}$ to $\sim 6\ \mu\text{s}$, as shown in Fig. 5(b), which unambiguously confirms the Q-switched nature of output laser. The maximized output pulsed energy is $\sim 150\ \text{nJ}$ for 22 kHz, which is similar to achieved results using MoS₂ [15]. In our platform, we think that the main factor to limiting the pulse energy is the optical damage threshold. The problem can be solved by composting MoS₂ nanoflakes with polymers. We did not observe any stable Q-switched phenomenon without MoS₂ SA. To obtain stable Q-switched laser, it needs either active or passive Q switches, and here we utilized MoS₂ thin film to operate as SA.

To achieve tunable fiber laser, we employed the translational stage as shown in Fig. 3(a) to stretch the MFC. As we can see clearly from Fig. 6(a), the output laser wavelength shift to shorter wavelength with increased strain of MFC. It should be noted that during the tuning process, the pump power is fixed at 30 mW, and the polarization controller is also kept constant. We can find that the shape of output spectrum change as strain

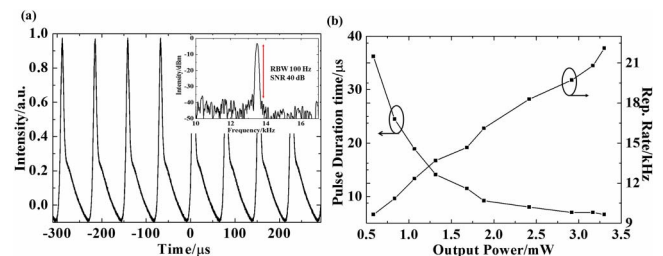


Fig. 5. Q-switched fiber laser characteristics. (a) The pulse train with launched pump power 60 mW. The inset is the corresponding RF spectrum. (b) Variation of repetition frequency and pulse duration time with output power.

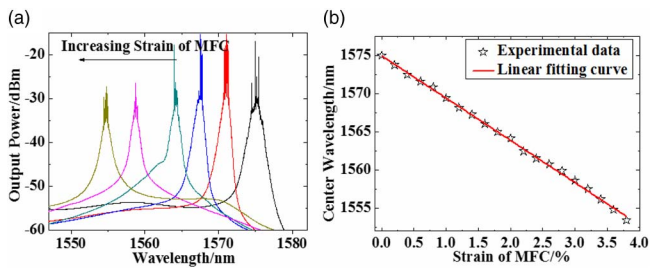


Fig. 6. Variation of optical spectrum with varied strain of MFC. (a) The blue shift of output spectrum of MFC as the strain increased. (b) Center wavelength shift dependence on the strain of MFC.

of MFC increased, which can be attributed to the wavelength-dependent gain ratio of our EDF and minor change of coupling ratio as illustrated in Fig. 3(c). Figure 6(b) shows in detail the wavelength tuning as the strain of MFC. We utilized Lorentz fitting to pick up the center wavelength of output spectrum. As we can see, the output laser wavelength monotonically decreased from 1575 to 1550 nm as the strain of MFC increased from 0% to 3.8%. The tuning sensitivity is as high as ~ 5.5 nm/(1% strain). When the strain increased further, in this part, larger than 3.8%, we observed multi-wavelength lasing phenomenon. By monitoring the output spectrum of MFC, we found that the coupling spectrum of MFC deteriorated. As a result, the lasing wavelength selecting functionality of MFC was damaged. Although here the MFC stretching technique inducing wavelength tuning does not cover the whole gain bandwidth of erbium-doped fiber, we believe that by further optimizing the structure of MFC, for example, the coupling length, diameter of MFC (coupling coefficient), etc., the problem may be overcome. Further, in principle, the in-line wavelength tuning technique can be easily expanded to other optical band, such as 1 μm , 2 μm , etc.

Here, we provided a new method to continuously tune the wavelength of *Q*-switched fiber laser based on few-layer MoS_2 . Thanks to the good quality of as fabricated SA, $\sim 29\%$ modulation depth has been achieved. By controlling the cavity loss through a strained MFC, we have demonstrated a *Q*-switched fiber tuning from 1550 to 1575 nm with a tuning sensitivity of ~ 5.5 nm/(1% strain). However, we should notice that this technique still has some problems, like the evident optical spectrum shape changed as the strain of MFC increased. By optimizing the structure of MFC, we believe optical spectrum shape problem can be solved, and the tuning range may cover the whole gain bandwidth of the erbium-doped fiber laser. Besides, by carefully designing the structure of MFC, it is promising to achieve multi-wavelength lasing, which has been observed in our laboratory. Finally, this technique can be readily applied to different optical-band fiber laser. The deduction is based on the basic principle of *Q*-switched fiber laser. The wavelength-tuning technique we used is by the means of controlling cavity loss based on microfiber coupling. It should be a universal method and independent of optical bands.

Funding. National Natural Science Foundation of China (NSFC) (61225026, 61322503, 61475069).

Acknowledgment. The authors thank Yue-hui Chen for helping Raman characterizations.

REFERENCES

1. K. S. Novoselov, A. K. Geim, S. Morozov, D. Jiang, Y. Zhang, S. Dubonos, I. Grigorieva, and A. Firsov, *Science* **306**, 666 (2004).
2. K. S. Novoselov, A. K. Geim, S. Morozov, D. Jiang, M. Katsnelson, I. Grigorieva, S. Dubonos, and A. Firsov, *Nature* **438**, 197 (2005).
3. A. K. Geim and K. S. Novoselov, *Nat. Mater.* **6**, 183 (2007).
4. B. Radisavljevic, A. Radenovic, J. Brivio, V. Giacometti, and A. Kis, *Nat. Nanotechnol.* **6**, 147 (2011).
5. K. F. Mak, C. Lee, J. Hone, J. Shan, and T. F. Heinz, *Phys. Rev. Lett.* **105**, 136805 (2010).
6. A. Splendiani, L. Sun, Y. Zhang, T. Li, J. Kim, C.-Y. Chim, G. Galli, and F. Wang, *Nano Lett.* **10**, 1271 (2010).
7. D. Xiao, G. B. Liu, W. X. Feng, X. D. Xu, and W. Yao, *Phys. Rev. Lett.* **108**, 196802 (2012).
8. K. F. Mak, K. He, J. Shan, and T. F. Heinz, *Nat. Nanotechnol.* **7**, 494 (2012).
9. H. Zeng, J. Dai, W. Yao, D. Xiao, and X. Cui, *Nat. Nanotechnol.* **7**, 490 (2012).
10. W.-T. Hsu, Z.-A. Zhao, L.-J. Li, C.-H. Chen, M.-H. Chiu, P.-S. Chang, Y.-C. Chou, and W.-H. Chang, *ACS Nano* **8**, 2951 (2014).
11. L. M. Malard, T. V. Alencar, A. P. M. Barboza, K. F. Mak, and A. M. de Paula, *Phys. Rev. B* **87**, 201401 (2013).
12. X. B. Yin, Z. L. Ye, D. A. Chenet, Y. Ye, K. O'Brien, J. C. Hone, and X. Zhang, *Science* **344**, 488 (2014).
13. S. Wang, H. Yu, H. Zhang, A. Wang, M. Zhao, Y. Chen, L. Mei, and J. Wang, *Adv. Mater.* **26**, 3538 (2014).
14. R. Woodward, E. Kelleher, R. Howe, G. Hu, F. Torrisi, T. Hasan, S. Popov, and J. Taylor, *Opt. Express* **22**, 31113 (2014).
15. Y. Huang, Z. Luo, Y. Li, M. Zhong, B. Xu, K. Che, H. Xu, Z. Cai, J. Peng, and J. Weng, *Opt. Express* **22**, 25258 (2014).
16. H. Liu, A.-P. Luo, F.-Z. Wang, R. Tang, M. Liu, Z.-C. Luo, W.-C. Xu, C.-J. Zhao, and H. Zhang, *Opt. Lett.* **39**, 4591 (2014).
17. J. Du, Q. Wang, G. Jiang, C. Xu, C. Zhao, Y. Xiang, Y. Chen, S. Wen, and H. Zhang, *Sci. Rep.* **4**, 6346 (2014).
18. H. Zhang, S. Lu, J. Zheng, J. Du, S. Wen, D. Tang, and K. Loh, *Opt. Express* **22**, 7249 (2014).
19. A.-P. Luo, M. Liu, X.-D. Wang, Q.-Y. Ning, W.-C. Xu, and Z.-C. Luo, *Photon. Res.* **3**, A69 (2015).
20. D. Popa, Z. Sun, F. Torrisi, T. Hasan, F. Wang, and A. Ferrari, *Appl. Phys. Lett.* **97**, 203106 (2010).
21. S. Lu, L. Miao, Z. Guo, X. Qi, C. Zhao, H. Zhang, S. Wen, D. Tang, and D. Fan, *Opt. Express* **23**, 11183 (2015).
22. Z. Yu, Y. Song, J. Tian, Z. Dou, H. Guoyu, K. Li, H. Li, and X. Zhang, *Opt. Express* **22**, 11508 (2014).
23. Z. Luo, Y. Huang, J. Weng, H. Cheng, Z. Lin, B. Xu, Z. Cai, and H. Xu, *Opt. Express* **21**, 29516 (2013).
24. Y. Chen, S.-C. Yan, X. Zheng, F. Xu, and Y.-Q. Lu, *Opt. Express* **22**, 2443 (2014).
25. L. Reekie, R. J. Mears, S. B. Poole, and D. N. Payne, *J. Lightwave Technol.* **4**, 956 (1986).
26. P. D. Humphrey and J. E. Bowers, *IEEE Photon. Technol.* **5**, 32 (1993).
27. M. B. Dines, *Mater. Res. Bull.* **10**, 287 (1975).
28. P. Joensen, R. Frindt, and S. R. Morrison, *Mater. Res. Bull.* **21**, 457 (1986).
29. C. Lee, H. Yan, L. E. Brus, T. F. Heinz, J. Hone, and S. Ryu, *ACS Nano* **4**, 2695 (2010).
30. K.-K. Liu, W. Zhang, Y.-H. Lee, Y.-C. Lin, M.-T. Chang, C.-Y. Su, C.-S. Chang, H. Li, Y. Shi, and H. Zhang, *Nano Lett.* **12**, 1538 (2012).